Chapter 3: Biodegradation of *p*-cresol by *Serratia marcescens* strain HL 1 in batch system: Process optimization, growth kinetics study, phytotoxicity and chlorophyll assessment

The content that is included in this chapter has been published.

***Jaiswal, V.K.**, Maurya, K.L., Sonwani, R.K., Singh, R.S., 2023. Biodegradation of p-cresol by Serratia marcescens strain HL 1 in batch system: Process optimization, growth kinetic study, phytotoxicity and chlorophyll assessment. Bioresour. Technol. Reports 22, 101426. https://doi.org/10.1016/j.biteb.2023.101426*

3.1. Introduction

The rapid growth of the industrialization has resulted in the generation of significant amount of effluents (Rea et al., 2022). The pollutants, namely, phenol and its derivatives (*p*-cresol, nitrophenols, chlorophenols, etc.), are the common waste pollutants found in waste effluents of petrochemical and chemical industries (Iliuta and Iliuta, 2022; Singh et al., 2017). These pollutants exert adverse impacts on the environment and human health. Among these, cresols compounds are considered most challenging pollutants due to their adverse impacts (Choquette-Labb´e et al., 2014). Depending on where the CH_3 group is located on the benzene ring, cresols are classified as ortho-, meta-, and para-cresols. These are highly soluble in water. Various industries, including petroleum refineries, pulp and paper mills, herbicides, fungicides, textile mills, explosive production, coal gasification plants, and coal conversion processes effluents contain large amount of phenolic compound (Xenofontos et al., 2016). Cresols can be found in up to 30 % of coke oven and coal conversion effluents (Bera et al., 2019). Coke oven effluent has a COD value between 1525 to 2450 mg L^{-1}, with phenolic compounds making up almost 80 % of the total COD (Panigrahy et al., 2020). However, because *p*-cresol is a highly toxic and carcinogenic pollutant, low *p*-cresol concentration significantly affects the nervous system, deep skin pigmentation, gastrointestinal bleeding, cardiovascular system, lungs, and kidneys (Kumar et al., 2018; Singh et al., 2017). *p*-Cresol can also be toxic to microbial cells while suppressing microbial aromatic ring cleavage (Panigrahy et al., 2020). The European Union has designated phenol as a "substance undesirable in excessive proportions." It has been determined that its concentration in water bodies, such as lakes and streams, shall not exceed 0.3 mg L^{-1} (Zuane 1997). United States Environmental Protection Agency (USEPA) classifies *p*-cresol as a priority pollutant Group C pollutant (possible human carcinogen) (Mahdavianpour et al., 2018). WHO (World Health Organization) has set the permissible limit 0.001 mg L^{-1} of *p*-cresol in drinking water (Singh et al., 2017). Ministry of Environment and Forest (MOEF) of the Government of India has limited the maximum permissible concentration of 1.0 mg L^{-1} *p*-cresol of industrial effluents for impervious release into ground waters (Zarei, 2018). *p*-Cresol concentration in wastewater must be below the permissible level reported by various environmental agencies. Previously, various physicochemical processes, namely adsorption (Bakas et al., 2014), chemical oxidation (Supandi et al., 2020), UV-visible irradiation (Khunphonoi and Grisdanurak, 2016),

ultrafiltration (Verma and Sarkar, 2018), catalytic ozonation (Ma et al., 2019), and membrane-based techniques (Hsiao et al., 2022) have been used for removal of *p*-cresol from wastewater. Most of these processes are associated with demerits such as high costs, susceptibility to secondary hazardous by-product production, and incomplete *p*-cresol conversion (Fu and Wang, 2011). In the last few decades, the biological methods based on biodegradation remain one of the most effective approaches due to their cost-effectiveness, ease of implementation, eco-friendly nature, and complete conversion of pollutants into innoxious compounds such as water and carbon dioxide through the microorganism (Sangwan and Dukare, 2018). Some microorganisms have been used for biodegradation of *p*-cresol **(Appendix 3 (a)).**

As per the literature review, minimal attention has been given to the biodegradation of *p*-cresol and its growth kinetics and phytotoxicity. Biodegradation kinetics plays an essential role in designing bioreactors. In this work, an effort has been given to isolate the potential bacterial species from activated sludge samples to degrade *p*-cresol. Central Composite Design (CCD) of Response Surface Methodology (RSM) was used to optimize the process variables, including pH, *p*-cresol concentration, and retention time (RT). In addition, kinetic parameters were evaluated by first-order, second-order (Grau model), and growth inhibition models. Phytotoxicity and chlorophyll assessment of *Vigna radiata* was studied for both treated and untreated *p*-cresol solution.

3.2. Materials and methods

3.2.1. Mineral salt medium (MSM) and chemicals

In this present study, *p*-cresol (99 %) was purchased from SigmaAldrich, Germany. Mineral Salt Medium (MSM) was prepared in double-distilled water. The composition of MSM was prepared as follows: $NaNO_3$ (4.0 g L^{-1}), KH_2PO_4 (1.75 g L^{-1}), Na_2HPO_4 (3.61 g L^{-1}), $MgSO_4{\cdot}7H_2O$ (0.2 g L^{-1}), $FeSO_4{\cdot}5H_2O$ (0.001 g L^{-1}), $CaCl_2{\cdot}2H_2O$ (0.05 g L^{-1}), $CuSO_4{\cdot}5H_2O$ (50 µg L^{-1}), $MnSO_4$ (10 µg L^{-1}), Na_2MoO_3 (10 µg L^{-1}) and modified with 3.0 g L^{-1} of yeast extract (Bera et al., 2019). MSM was sterilized for 15 min at 120 ^oC and 15 psi. MSM was mixed with stock solution (1000 mg L^{-1}) of *p*-cresol to prepare the synthetic wastewater. To keep the pH of the synthetic wastewater constant, NaOH (0.1 M) and HCl (0.1 M) were employed.

3.2.2. Isolation of pure strain and acclimatization

The bacterial species were isolated from the activated sludge acquired from the IOCL (Indian Oil Corporation Limited) refinery, Mathura (UP), India. To keep the pH of the synthetic wastewater constant, NaOH (0.1 M) and HCl (0.1 M) were employed. The isolation technique used in this study has been discussed elsewhere (Sonwani et al., 2019). In brief, 100 mL of MSM and 50 mg L^{-1} of *p*-cresol were added to 250 mL conical flask along with 5 g of activated sludge sample. The conical flask was then incubated at room temperature and 120 rpm in a rotatory shaker for 7 days. After 7 days of incubation, the new MSM media with 100 mg L^{-1} of *p*-cresol concentration was inoculated with 20 mL of the previously acclimatized sample. This process was carried out by moderately increasing *p*-cresol concentration. Acclimatized bacteria were used as an inoculum in the stirred conical flask for *p*-cresol biodegradation.

3.2.3. Bacterial identification

Triyat Scientific in Nagpur, India, characterized the viable bacterial species. The DNA was amplified using polymerase chain reaction (PCR) with universal forward (27F-5′ GGATGAGCCCGGCCTA3′) and reverse (11492R-5′ CGGTGTGTACAAGGCCCGG3′) primers. For the PCR, thermal cycling conditions were as follows: denaturation at 94 °C for 1 min, initial denaturation at 94 °C for 3 min, extension at 72 °C for 2 min, and annealing at 50 °C for 1 min. The sequencing was conducted using the ABI 3730xl sequencer. The NCBI similarity search tool was used to align the 16S rRNA sequence. Accession number (EU371058.1) was obtained from Genbank. The phylogenetic query sequence analysis with closely related blast results sequence was performed. MEGA7 (Molecular Evolutionary Genetics Analysis Tool) software was used to construct a neighbor-joining phylogenetic tree **(Appendix 3 (b)).**

3.2.4. Analytical methods

OD (optical density) was determined by measuring the absorbance at 600 nm using UV/VIS spectrophotometer (PerkinElmer Lambda 25 UV/VIS Spectrometer). To analyze residual *p*-cresol concentration, HPLC (High Performance Liquid Chromatography) (UFLC Shimadzu, Japan) equipped with C-18 (4.6 mm × 250 mm × 5 mm, reverse phase, Inert Sustain) column at 30 °C and UV detector set at 275 nm, was used. The solvent made of methanol and water (80:20

v/v) was used as carrier with flow rate of 1.0 mL min^{-1}. The samples were centrifuged for 15 min at 5000 rpm before being filtered with a syringe filter (0.20 µm).

3.2.5. Growth kinetics for biodegradation of *p*-cresol

The kinetic model parameters were evaluated by observing the biomass growth rate at various initial substrate concentrations in batch experiments. An equation illustrating the relationship between the specific growth rate and the substrate concentration is one of the most crucial factors to evaluate growth kinetics of microorganisms.

$$\frac{dX}{dt} = \mu \times X \quad \text{(3.1)}$$

or,

$$\mu = \frac{1}{X}\frac{dX}{dt} \quad \text{(3.2)}$$

Solving equation (3.2) from t = 0 to t = t

$$\mu = \frac{\ln(X_t) - \ln(X_0)}{t - t_0} \quad \text{(3.3)}$$

Where X_t(t = t) and X_0(t = 0) indicates biomass conc.

Eq. (3.1) was utilised to calculate the cell-specific growth rate in log phase. The slope of the graph between $\ln\left(\frac{X}{X_0}\right)$ and Δt was used to get the value of μ. Cell concentration (X) was measured using UV-VIS spectrophotometer at 600 nm (Bera et al., 2019; Swain et al., 2020). Since bacterial growth was inhibited at higher *p*-cresol concentration, various substrate inhibition models could be employed to calculate various kinetic parameters.

Andrew-Haldane model

$$\mu = \frac{\mu_{max} \times S}{K_S + S + \frac{S^2}{K_I}} \quad \text{(3.4)}$$

Monod model

$$\mu = \frac{\mu_{max} \times S}{K_S + S} \quad \text{(3.5)}$$

Aiba model

$$\mu = \frac{\mu_{max} \times S}{K_S + S} \times \exp\left(-\frac{S}{K_S}\right) \quad \text{(3.6)}$$

Edward model

$$\mu = (\mu_{max} \times S) \times \left(exp \times \left(-\frac{S}{K_I}\right) - exp \times \left(-\frac{S}{K_S}\right)\right) \quad \text{(3.7)}$$

Yano model

$$\mu = \frac{(\mu_{max} S)}{K_S + S + \left(\frac{S^2}{K_I}\right) \times \left(1 + \frac{S}{K}\right)} \quad \text{(3.8)}$$

Webb model

$$\mu = \frac{(\mu_{max} \times S) \times \left(1 + \frac{S}{K}\right)}{\left(K_S + S + \left(\frac{S^2}{K_I}\right)\right)} \quad \text{(3.9)}$$

The value of bio-kinetic coefficients, such as μ_{max} (maximum specific growth rate, h^{-1}), K_I (substrate-inhibition constant, mg L^{-1}), K_S (substrate-affinity constant, mg L^{-1}), and K (Yano and Webb model constant) were obtained by MATLAB R2017b.

3.2.6. Process variable optimization using response surface methodology

RSM with CCD is an effective technique for exploring the relationship between multiple process variables and their results. The RSM technique has examined how process variables like pH, concentration, and temperature interact (Umar et al., 2017). The Design-Expert software system (Version13, Stat-Ease Inc., Minneapolis, USA) was used to evaluate the interaction effect of independent process variable parameters. 3D surface and contour graphs were plotted to investigate how variables affect the response. Optimal conditions were anticipated based on the p (probability) and F (Frisher's) values. **Table 3.1** shows the list of independent process variable selected for biodegradation of *p*-cresol.

Table 3.1. : Independent process variable for biodegradation of *p*-cresol

Factor	Name	Units	Minimum	Maximum	Mean
A	pH		5.00	10.00	7.50
B	*p*-cresol conc.	mg L^{-1}	20.00	100.00	60.00
C	RT	h	24.00	72.00	48.00

conc.: Concentration; RT: Retention time

A polynomial equation of second order was used to analyze the experimental data as given bellow:

$$Y= \alpha_0 + \alpha_1 A + \alpha_2 B + \alpha_3 C + \alpha_1\alpha_2 AB + \alpha_2\alpha_3 BC + \alpha_1\alpha_3 AC + \alpha_{11} A^2 + \alpha_{22} B^2 + \alpha_{33} C^2 \quad (3.10)$$

Where Y is the response variable ((%) removal), A, B, and C are the pH, *p*-cresol concentration, and RT, respectively. α_0 is an offset term; α_1, α_2, and α_3 are regression coefficients for a linear function. $\alpha_1\alpha_2$, $\alpha_2\alpha_3$, and $\alpha_1\alpha_3$ are regression coefficients for the interaction effect α_{11}, α_{22}, and α_{33} are regression coefficients for the quadratic function. After performing experiments, the predicted and adjusted regression coefficient (R^2) value, response plot, and variance analysis (ANOVA) were used to calculate *p*-cresol removal efficiency (%).

3.2.7. Kinetic model

Kinetic models can help predict bioreactor performance (Swain et al., 2020). It is generally based on the pH of wastewater, retention time, and concentration. The batch experiment was performed at optimized predicament (pH 7.5, RT = 48.0 h, and *p*-cresol concentration = 60 mg L^{-1}). The rate kinetics of *p*-cresol was calculated using first-order and second-order (Grau model) models in this study (Swain et al., 2020).

3.2.7.1.First-order kinetic model

A first-order kinetic model was used to express the *p*-cresol removal in the batch experiment (Brink et al., 2017; Swain et al., 2020) as follows:

$$\frac{dS}{dt} = -k \times X \times S \quad (3.11)$$

Where S is the *p*-cresol concentration (mg L^{-1}) at any time $t = t$ within the stirred conical flask, t is the retention time (h), k is the rate constant for the first order (L mg VSS^{-1} h^{-1}), and X is the biomass concentration (mg L^{-1}). S cannot be determined by directly by solving **Eq. (3.11)** since S and X is both functions of time. As a result, in **Eq. (3.11),** an average biomass concentration ($\bar{X}$) is used and clumped with k to give the new rate law as follows

$$\frac{S_o - S}{t} = k_1. \quad (3.12)$$

k_1 is the clumped first-order kinetic parameter, which could be calculated by analyzing the slope of the graph between $\frac{S_0 - S}{t}$ and s.

3.2.7.2.Second-order kinetic model (Grau model)

Eq. (3.13) represents the second-order kinetic for the removal of *p-cresol*

$\frac{dS}{dt} = -k_s \times X \times S^2$ .....(3.13)

Wherek_s (L^2 $gVSS^{-1}$ $gCOD^{-1}$ h^{-1}) is the rate constant for the second-order kinetic, based on the initial substrate concentration of the substrate and average biomass density within the stirred conical flask (Swain et al., 2020).

In the above equation, X is unknown and variable (function of time); ($\bar{X}$) an average biomass concentration is accustomed in **Eq. (3.13)** and clumped with K_s.

$\frac{dS}{dt} = -(k_s. \times (\bar{X})) \times S^2 = -k_2 \times S^2$ .....(3.14)

Integrating and linearization the **Eq. (3.14)**

$\frac{S_0 t}{S_0 - S} = \frac{1}{k_2 S_0} + t$ .....(3.15)

Where S_0 (mg L^{-1}) is the initial concentration of the substrate, and k_2 (L mg.VSS h^{-1}) is the clumped rate constant for the second-order. The removal efficiency $\frac{S_0 - S}{S_0}$ demonstrated as E. Yet again, the constant n denotes $\frac{1}{k_2 S_0}$ in **Eq. (3.15).**

$\frac{t}{E} = n.t + m$ .....(3.16)

The second-order kinetic parameters are n and m (h), calculated by evaluating the slope and intercept of the graph t/E versus t.

3.2.8. Phytotoxicity assessment

Assessment of phytotoxicity revealed how the pollutant adversely affected the plant growth and its metabolisms. Plant metabolism and growth are influenced due to disrupted physiological functioning, such as seed germination, photosynthesis, water and nutrient accumulation. The phytotoxicity analysis was carried out using *Vigna radiata* (mung bean) seeds. *Vigna radiata* was soaked with 1% NaClO for 5 min and then washed thrice through double distilled water to avoid any fungal infections (Ahemad et al., 2021). Three petri dishes were prepared with double layer, cotton layer with a thickness of 5 mm at the bottom and a Whatman filter paper at the bottom and at the top. Seven seeds of *Vigna radiata* were placed between these two layers and provided 5 mL of control water (double distilled water), treated and untreated samples and irrigated with respective water at regular time intervals. Each plate was placed at 30 ^{o}C for

germination. When the radicle length was at least 2 mm, a seed was deemed to have germinated (Luo et al., 2018). % germination was calculated based on 2 days of observation and % relative root growth (% RRG), % relative seed germination (% RSG), phytotoxicity index (PI) and % germination index (% GI) was calculated based on 7 days of observation.

$$\% \text{ RRG} = \frac{root\ length\ of\ sample}{root\ length\ of\ control\ sample} \times 100 \quad (3.17)$$

$$\% \text{ RSG} = \frac{germination\ of\ seed\ in\ sample}{germination\ of\ seed\ in\ control\ sample} \times 100 \quad (3.18)$$

$$\text{PI} = 1 - \frac{root\ length\ of\ sample}{root\ length\ of\ control\ sample} \quad (3.19)$$

$$\% \text{ GI} = \frac{RRG \times RSG}{100} \quad (3.20)$$

3.2.9. Chlorophyll content assessment

Chlorophyll is a crucial pigment that absorbs light energy for photosynthesis and increases cell biomass under optimum conditions (Khorshidi et al., 2022). The main components of photosynthesis in land plants and green algae are chlorophylls a and b. Chlorophyll b, just on the other hand, is a supplementary pigment that absorbs energy and transfers it to chlorophyll a (Tanaka and Tanaka, 2011). Chlorophyll b is necessary for stabilizing the major light-harvesting chlorophyll-binding proteins (Kume et al., 2018).

Dimethyl sulfoxide (DMSO), a solvent with amphiphilic qualities that quickly diffused through the membrane and denatured the protein by displacing the surrounding water, was used to extract chlorophyll from *Vigna radiata* leaves. 0.1 g of leaves were cut into small pieces and soaked in 10 mL DMSO solvent, incubated at 60-70 ^{o}C for 1 h, followed by 30 min cooling at room temperature. The collected sample was centrifuged and filtered with 0.20 µm filter paper. Absorbance was measured by SL 159 UV-VIS spectrophotometer, using DMSO as blank. Chlorophyll a and b concentrations and total chlorophyll were calculated in terms of mg (g fresh weight (F.W))$^{-1}$ (Manolopoulou et al., 2016). It was calculated by the formula suggested by the Barnes et al. 1992.

Chlorophyll a (mg g^{-1} F.W) = (14.85 ab_{665} – 5.14 ab_{648}) ……..……..……..(3.21)

Chlorophyll a (mg g^{-1} F.W) = (25.48 ab_{665} – 7.36 ab_{648}) ……..……..(3.22)

Total chlorophyll (mg g^{-1} F.W) = (7.49 ab_{665} + 20.34 ab_{648}) ..……..……...(3.23)

3.3. Results and discussions

3.3.1. Growth kinetic study

The specific growth of microorganisms at different concentration of *p*-cresol was calculated by plotting a graph between $\ln(\frac{X}{X_o})$ versus t. Variation in specific growth with substrate conc (*p*-cresol conc.) was shown in **Fig. 3.1.** Five different substrate-inhibition kinetic models such as Andrew-Haldane model, Monod model, Aiba model, Edward model, Yano model, and Webb model were used to examine the experimental data. ln MATLABR2017b, the various models were analyzed using non- linear regression analysis to perform the curve fitting. The summary bio- kinetic parameters and the coefficient of correlation (R^2) are represented in **Table 3.2.** Data fitted with the Andrew-Haldane model showed higher R^2 value of 0.98. The specific growth rate (μ), substrate affinity constant (K_s), and substrate inhibition constant (K_I) were obtained to be 0.2 h^{-1}, 22.5 mg L^{-1}, and 76 mg L^{-1}, respectively. The growth of microorganisms increased with concentrations up to 75 mg L^{-1}, and beyond that, the growth was reduced due to substrate inhibition (**Fig. 3.1**). The metabolic activity of bacteria is adversely affected by the high *p*-cresol concentration.

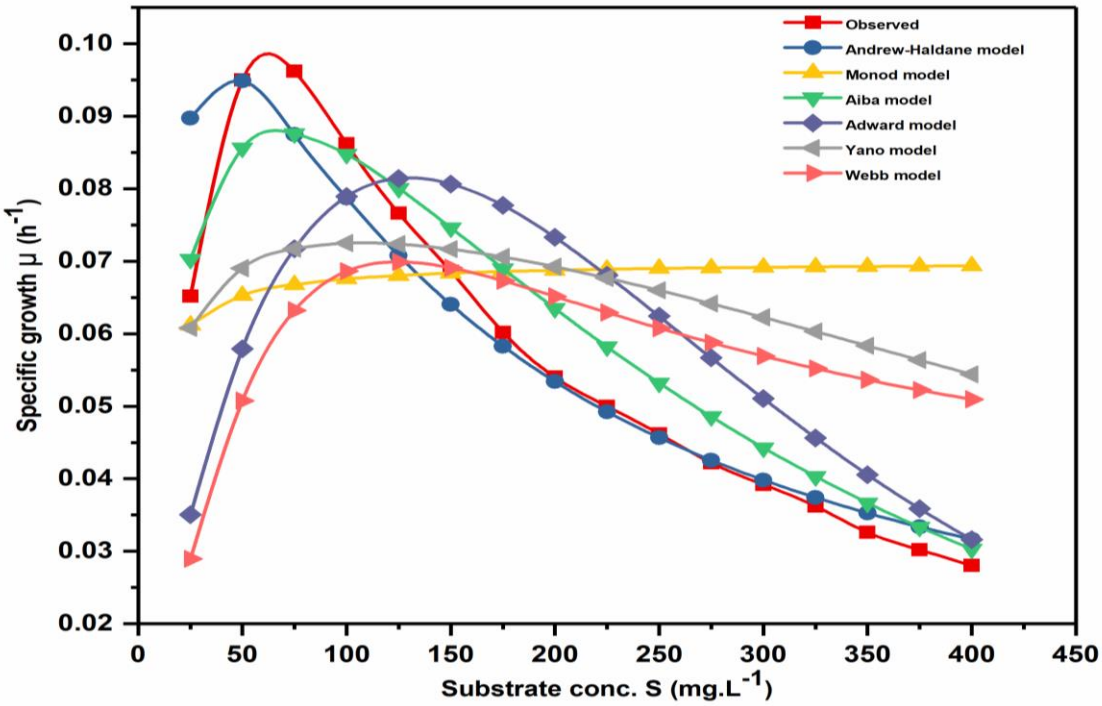

Fig. 3.1. Plot represent experimental specific growth rate and different model predicted growth rate of *Serratia marcescens* strain HL 1 (EU371058) at various initial *p*-cresol conc.

Serratia marcescens HL 1 (EU371058) has a maximum specific growth rate of 0.2 h^{-1}, which is higher than the maximum specific growth rates of *A. chlorophenolicus* A6, *Rhodococcus erythropolis* M1, and bacterial consortium (Bera et al., 2017; Goswami et al., 2002; Sahoo et al., 2011).

Table 3.2. : Bio-kinetic parameters based on numerous inhibition models

Kinetic model	μ_{max} (h^{-1})	K_S (mg L^{-1})	K_S (mg L^{-1})	K (mg L^{-1})	R^2
Andrew-Haldane model: $\mu = \frac{(\mu_{max} \times S)}{(Ks+S+(\frac{S^2}{K_I}))}$	0.2	22.5	76	-	0.98
Monod model: $\mu = \frac{(\mu_{max} \times S)}{(K_S+S)}$	0.07	3.6	-	-	0.69
Aiba model: $\mu = \frac{(\mu_{max} \times S)}{(K_S+S)} exp(-\frac{S}{K_I})$	0.16	26.5	250	-	0.89
Edward model: $\mu = (\mu max \times S) \times (exp \times \left(-\frac{S}{K_I}\right) - exp \times \left(-\frac{S}{K_S}\right))$	0.0017	3.6	130.33		0.91
Yano model: $\mu = \frac{(\mu_{max} \times S)}{(Ks+S+(\frac{S^2}{K_I}) * (1+\frac{S}{K})}$	0.082	8.56	5000	78.81	0.74
Webb model: $\mu = \frac{(\mu_{max} \times S) \times (1+\frac{S}{K})}{(K_s+S+(\frac{S^2}{K_I}))}$	1.0169	928.32	10.36	362.36	0.90

3.3.2. Process variable parameter optimization

For the optimization investigation, the independent process variable parameters pH (5–10), *p*-cresol concentration (20–100 mg L^{-1}), and RT (24-72 h) were selected. The removal efficiency (%) of *p*-cresol was taken as the response variable. Total 20 experiments were performed to investigate the correlation between the process independent variables and the responses. A

summary of the results is listed in **Table 3.3.** Considering the validation of various regression models, it was found that the quadratic model fit perfectly the collected data. **Table 3.4.** provided an overview of the values for adjusted R^2 and predicted R^2 values evaluated using quadratic models. The adjusted R^2 values were found to be 0.99.

Table 3.3.: Experimentally obtained responses at different operating conditions used in RSM optimization

Run	Factor A	Factor B	Factor C	Response 1
	A: pH	B: *p*-cresol conc. (mg L^{-1})	C: RT (h)	% Removal efficiency
1	7.5	60	48	86.32
2	10	60	48	22.63
3	7.5	60	48	85.36
4	10	100	72	18.32
5	7.5	20	48	90.32
6	10	100	24	10.32
7	5	100	24	7.63
8	7.5	60	48	81.32
9	7.5	60	48	82.36
10	7.5	60	48	84.36
11	10	20	72	32.32
12	5	20	24	10.32
13	10	20	24	16.36
14	7.5	100	48	72.36
15	5	20	72	33.62
16	5	60	48	16.82
17	7.5	60	48	82.36
18	5	100	72	15.63
19	7.5	60	72	94.36
20	7.5	60	24	76.32

Similarly, the predicted R^2 values were found to be 0.97. The quadratic model was acceptable if the acquired R^2 values were greater than 0.9. It is reported that the model shows the coefficient of correlation (R^2) of more than 0.8 are well fitted with experimental data (Sonwani et al., 2019; Gusain et al., 2016). Graphical plot between predicted and actual values is shown in Appendix **(Appendix 3 (c)).** The quadratic model fits the experimental data well, and the effect of the variables on response can be expressed as a quadratic **Eq. (3.12).** The model square terms (A^2) and linear coefficients (B and C) were more significant ($p<0.05$) than the other coefficients

(**Table 3.5**). The interactions between the variables A, B, and A, C were insignificant, while the interaction between the variables B and C was significant ($p< 0.05$). The quadratic model was sufficient for investigating response and variable correlation, as shown by the regression model's overall significance ($p< 0.0001$). Silva et al. (2018) reported higher Fisher's F value and lower p indicate that the model has a significant coefficient.

$$Y = 83.23 + 1.59A - 5.87B + 7.33C + 0.0800AB - 0.9175AC - 2.91BC - 64.08A^2 - 2.47B^2 + 1.53C^2 \quad (3.24)$$

Table 3.4.: Brief summary of model fit statistics

Std. Dev.	Mean	C.V.%	R^2	Adjusted R^2	Predicted R^2	Adeq Precision
2.62	50.72	5.17	0.9969	0.9940	0.9783	46.7841

%C. V.: %Coefficient of variance

Table 3. 5.: Response 1: Summary of the ANOVA for the quadratic model

Source	Sum of Squares	df	Mean Square	F- value	p-value	
Model	21895.52	9	2432.84	353.67	< 0.0001	Significant
A-pH	25.38	1	25.38	3.69	0.0837	
B-*p*-cresol concentration	344.33	1	344.33	50.06	< 0.0001	
C-RT	537.29	1	537.29	78.11	< 0.0001	
AB	0.0512	1	0.0512	0.0074	0.9330	
AC	6.73	1	6.73	0.9790	0.3458	
BC	67.63	1	67.63	9.83	0.0106	
A^2	11293.62	1	11293.62	1641.80	< 0.0001	
B^2	16.77	1	16.77	2.44	0.1495	
C^2	6.45	1	6.45	0.9370	0.3559	
Residual	68.79	10	6.88			
Lack of Fit	45.45	5	9.09	1.95	0.2411	not significant
Pure Error	23.34	5	4.67			
Cor Total	21964.31	19				

3.3.3. Effect of process independent variables on removal efficiency

3.3.3.1. Effect of concentration and pH

Fig. 3.2. shows the 3-D surface and contour plots of interacting factors such as pH, initial *p*-cresol concentration, and retention time against *p*-cresol removal efficiency. A very substantial interaction between pH and *p*-cresol concentration was revealed by the elliptical profile of the contour plot **(Fig. 3.2.(a, b)).** The *p*-cresol removal efficiency in stirred conical flask was reduced under highly acidic and alkaline medium. It may be due to inhibition of enzyme activity under highly acidic or alkaline conditions, which subsequently reduces the removal efficiency (Sutar et al., 2019). The optimum pH for *p*-cresol removal was found to be around 7.5. Previous researchers have reported that the neutral pH was ideal for the biodegradation of organic pollutants (Sonwani et al., 2020; Kureel et al., 2017). Similarly, the maximum *p*-cresol removal of 90.32 % was achieved at low concentration (20 mg L^{-1}), pH 7.5, and retention time of 48 h. However, the *p*-cresol removal efficiency decreased with increasing *p*-cresol concentration reaching 72.36 % at 100 mg L^{-1}, pH 7.5, and retention time (48 h). Sonwani et al. (2021) have reported the pH of 7.0 was suitable for maximum biodegradation of pollutant in moving bed biofilm reactor. The decrease in removal efficiency at higher concentration was probably due to limiting substrate inhibition. Swain et al. (2021) have studied the effect of 4-Chlorophenol concentration on its removal efficiency in a packed bed bioreactor. They reported that the 4-Chlorophenol removal efficiency was significantly decreased beyond 50 mg L^{-1} of initial 4-Chlorophenol.

3.3.3.2. Effect of retention time and pH

Fig 3.2.(c, d) illustrates the combined impact of RT and pH on *p*-cresol removal efficiency. The pH varied from 5.0 to 10. The removal efficiency of *p*-cresol increased with increasing pH up to 7.0 and further increasing the pH level, the removal efficiency started to decrease. At pH 7.0, the maximum removal efficiency of 94.3% was achieved with initial *p*-cresol of 60 mg L^{-1} and RT of 72 h. Bacteria produce enzymes with ionic groups on their active site and these ionic groups must be in the viable state (acid or base) for *p*-cresol biodegradation. As the pH changes, the ionic form of the active surface activity changes, reducing enzyme activity and thus removal efficiency. At optimized pH (7.5), the removal efficiency of *p*-cresol was significantly enhanced

by increasing the RT at a fixed concentration (60 mg L^{-1}). The increase in removal efficiency with increasing RT may be due to sufficient residence for growth of microorganisms in stirred conical flask.

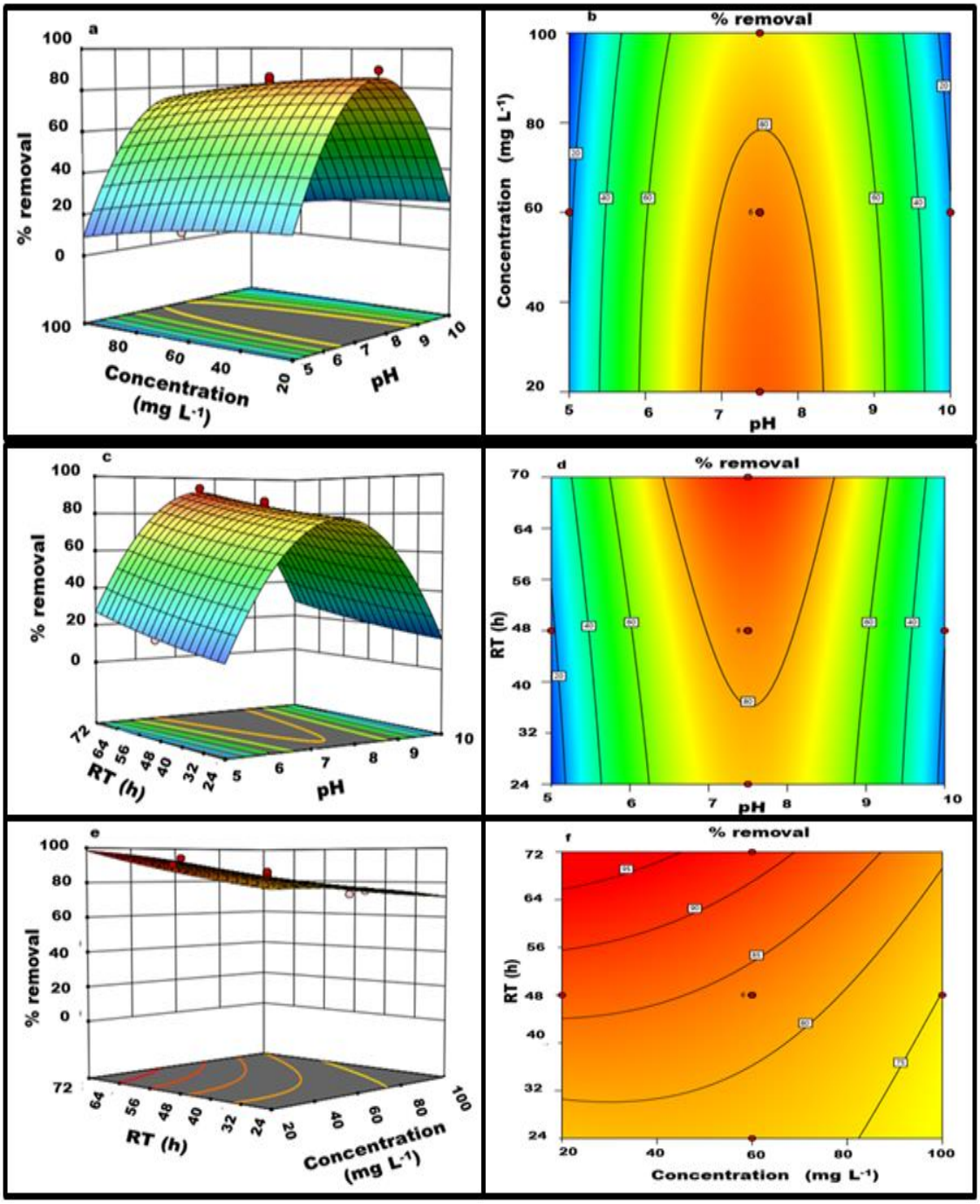

Fig. 3.2. Surface and contour plot of PC % removal efficiency; (a, b) effect of *p*-cresol conc. and pH; (c, d) effect of RT and pH; and (e, f) effect of RT and pH

3.3.3.3. Effect of retention time and concentration

Fig. 3.2. (e, f) demonstrates the simultaneous effect of RT and concentration on the removal efficiency. The *p*-cresol removal efficiency was increased with increasing RT from 24 h to 72 h. At high retention time, the microorganisms get sufficient time to interact with substrate and subsequently degrade the substrate effectively. For example, the *p*-cresol removal efficiency of 82.36% was observed in 48 h retention time, whereas the removal efficiency increased with RT and reached 94.36% at RT = 72 h and pH 7.5. These results revealed that an increased RT in stirred conical flask causes a significant amount of biomass generation. However, removal efficiency was decreased with increasing concentration. The decreased removal efficiency at high *p*-cresol concentration was due to the substrate inhibition and *p*-cresol toxicity to biomass. The high substrate concentration takes much longer to degrade in the bioreactor (Basak et al., 2019). According to Banerjee and Ghoshal (2016), the removal efficiency of phenol was decreased significantly due to the short residence time. In another study, Mohanty and Jena (2017) studied the effect of initial phenol concentration on its removal efficiency and reported that high removal efficiency was obtained at low *p*-cresol concentration due to the high tolerance limit against the toxicity of the substrate.

3.3.4. Kinetic Study

3.3.4.1. Model of first-order kinetic

The graph between $\left(\frac{S_0 - S}{t}\right)$ and (S) were utilized to evaluate the kinetic constants **(Fig. 3.3. (a)).** The clumped first-order kinetic constant (k_1) for *p*-cresol degradation was obtained as 0.0046 h^{-1}. The average biomass concentration was 2.3 g VSS L^{-1} obtained in batch experiment. The corresponding first-order rate constant was 0.002 L g VSS^{-1} h^{-1} evaluated from **Eq. (3.12).** The correlation coefficient (R^2) was calculated to be 0.99 and the average degradation rate of *p*-cresol was found 8.6 × 10^{-4} $g_{p\text{-cresol}}$ g VSS^{-1} h^{-1}. Zhang et al. (2020) used bacterial consortia for chloramphenicol biodegradation and reported that a first-order decay model fit.

3.3.4.2. Model of second-order kinetic

The experimental data fitted with second-order model is shown in **Fig. 3.3. (b).** The unknown kinetic parameters (n and m) can be obtained from the slope and intercept of graph between t/E

versus t. The kinetic parameter (i.e., n) was found to be 0.15. Similarly, the value of m was determined to be 72.39 (h). The clumped second-order rate constant (k_2) for *p*-cresol was obtained as 0.000457 L^2 g VSS^{-1} $gCOD^{-1}$ h^{-1}. The correlation coefficient (R^2) was calculated to be 0.88.

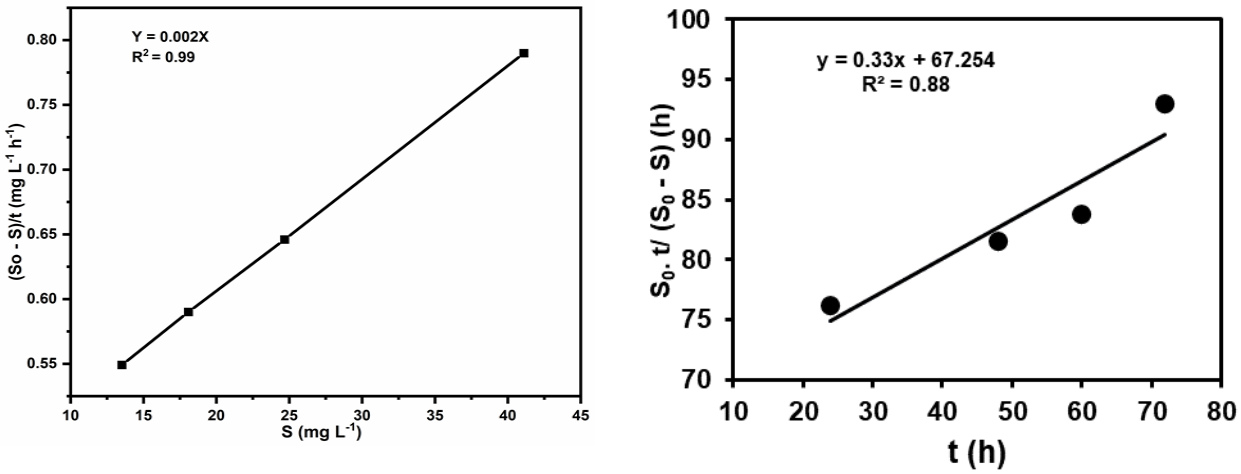

Fig. 3.3 (a) First-order kinetic model plot for *p*-cresol removal and (b) Second-order kinetic model plot for *p*-cresol removal

3.3.5. FTIR analysis

FTIR spectrum of biodegraded *p*-cresol shows the functional groups present in the solution (**Appendix 3(d)).** The spectra obtained at 3452 cm^{-1} may be due to intermolecular O-H stretching of the phenols, hydroxyls or carboxyl (Xue et al., 2015). The carbonyl group (C=O) vibrations in the carboxylic and ester group are responsible for the peak at about 1629 cm^{-1}, while the peak at about 1047 cm^{-1} is due to C-O-C vibrations (Shen et al., 2023). The bands in the region 1375–1350 cm^{-1} were identified by the C-H symmetric and asymmetric deformations in methyl and phenolic alcohol or by the C–H vibration in alkanes (Bledzki et al., 2010). The saturated ester bond of C–O groups is represented by the peak in the FTIR spectrum at around 1277 cm^{-1} (Kanavaki et al., 2021).

3.3.6. Bacterial toxicity

The bacterial toxicity assessment was carried out based on the previously published articles (Chaturvedi et al., 2021). Luminous bacteria were received from the National Centre for Microbial Resource (Pune, India) and cultivated in LB broth (Luria Bertani broth) for

bioluminescence toxicological analysis. Bacterial cultures with optical densities were utilized to analyse the bacterial toxicity. 1 mL of *Pseudomonas fluorescens* was added to 5 mL of each sample, i.e., distilled water as control, continuous system (CS), batch system (BS) and without degraded (WD) sample. For acute and chronic toxicity, samples were taken 30 min and 24 hr after inoculation with *Pseudomonas fluorescens*. The term % bioluminescence inhibition was defined as:

$$\% \text{ Bioluminescence inhibition} = \frac{Control\ sample\ intesity - Sample\ intensity}{Control\ sample\ intensity} \times 100 \ldots\ldots\ldots\ldots\ldots\ldots (4.4)$$

The bioluminescence intensities were expressed as counts per seconds.

3.3.7. Phytotoxicity assessment

Vigna radiata was used to analyze phytotoxicity for control, treated and untreated samples. A pictorial representation of seed germination and shoot and root growth is shown in appendix (**Appendix 3 (e)).** The result observed after 7 days of observation is presented in **Table 3.6.** It was observed that the difference between the root and shoot length of seeds compared to control is slightly less but significantly higher than untreated water and PI value of treated sample is much better than untreated sample. However, GI value is closer to control seeds. Higher the GI values higher the rate of germination. After observing different parameter values, which are essential for the assessment of the growth of seeds, we can conclude the treated sample can be used to irrigate the *Vigna radiata* seeds field.

Table 3.6.: Summary of toxicity assessment of *p*-cresol solution on *Vigna radiata* seeds in control, treated and untreated sample

Sample	Root length (cm)	Shoot length (cm)	% RRG	% RSG	PI	% GI
Control	3.02 ± 0.16	10.0 ± 0.14	100	100	0	100
Treated	2.75 ± 0.15	9.30 ± 0.11	93.33	85.71	0.07	79.99
Untreated	2.42 ± 0.11	8.44 ± 0.37	83.33	57.14	0.18	47.61

% RRG: % relative root growth; % RSG: % relative seed germination; PI: phytotoxicity index; % GI: % germination index

3.3.8. Chlorophyll a, b and total chlorophyll assessment

The Chlorophyll a and b concentrations and total chlorophyll were analysed based on the leaves of *Vigna radiata* over 7 days of observation. A summary of observed values has been presented

in **Table 3.7.** Chlorophyll a, chlorophyll b and total chlorophyll content were higher in treated water-inoculated seeds than in untreated water-inoculated seeds. Higher values of chlorophyll a, irrigated with treated water compared to untreated water, enhanced the photosynthesis process and improved the osmotic stress.

Table 3.7. Summary of chlorophyll assessment of *Vigna radiata* seeds in control, treated and untreated sample

Sample	Chlorophyll a (mg (g F.W)$^{-1}$)	Chlorophyll b (mg (g F.W)$^{-1}$)	Total Chlorophyll (mg (g F.W)$^{-1}$)
Control	10.40 ± 0.23	18.31 ± 0.15	12.57 ± 0.18
Treated	9.13 ± 0.16	16.05 ± 0.13	10.68b ± 0.16
Untreated	5.13 ± 0.11	9.05 ± 0.12	6.54 ± 0.21

3.4. Conclusions

An isolated viable bacterial strain (*Serratia marcescens* strain HL 1 (EU371058)) was employed in a series of batch studies to degrade *p*-cresol from wastewater. Various environmental parameters such as *p*-cresol concentration, pH, and retention time were optimized using CCD of RSM and optimum conditions were found to be 60 mg L^{-1}, 7.5, and 48 h, respectively. Growth inhibition kinetic models were employed to evaluate the bio-kinetic coefficients. With a correlation coefficient value of 0.98, Haldane's model provided the best fit among these models. Furthermore, first-order model was found to predict *p*-cresol degradation kinetics successfully and accurately. Phytotoxicity and chlorophyll assessment reveal that treated water can be used for irrigation purposes. This study can further be extended to treat the wide range of pollutants from wastewater.

Chapter 4: Construction and performance assessment of Recirculating packed bed biofilm reactor (RPBBR) for effective biodegradation of *p*-cresol from wastewater

The content that is included in this chapter has been published.

Jaiswal, V.K., Sonwani, R.K., Singh, R.S., 2023. Construction and performance assessment of Recirculating packed bed biofilm reactor (RPBBR) for effective biodegradation of p-cresol from wastewater. Bioresour. Technol. 384, 129372. https://doi.org/10.1016/j.biortech.2023.129372

4.1. Introduction

The inorganic and organic pollutants released from industries such as chemicals, petrochemicals, coking plants, paper mills are considered as a severe concern worldwide (Tiwari et al., 2023). Among the various pollutants, phenolic compounds are generally found in various industrial effluents involved in the production of herbicides, coke ovens, and coal conversion operations (Jaiswal et al., 2023). Furthermore, it has been reported that the wastewater from some of these industries often released into the soil and contaminates nearby water supplies and agricultural fields (Panigrahy et al., 2020). The phenolic chemical 4-methyl phenol (*p*-cresol) is a natural substance found in crude oil, and human/animal urine (Gonzalez-Blanco et al., 2012). Severe exposure to phenolic compounds damages the heart, liver, kidney, and neurological system (Shim et al., 2019; Singh et al., 2022a). The phenolic compound is considered one of the **"**substances undesirable in excessive proportions**"** by the European Union (Xenofontos et al., 2016). The World Health Organization (WHO) has established a permissible limit of 0.001 mg L^{-1} to regulate the amount of *p*-cresol compounds in drinking water (WHO, 1963). Therefore, the effluent containing phenolic compound must be treated to an adequate level before being discharged into open water bodies to prevent severe water pollution due to its toxicity. These pollutants are generally eliminated by electrolytic oxidation, catalytic oxidation, photocatalytic degradation, and adsorption (Mahdavianpour et al., 2018). However, these treatments are expensive and by-products formed during the process may be more toxic than the original pollutants (Martinkova et al., 2016). However, microbial remediation is favoured over conventional physicochemical techniques due to their environmental friendliness, cost-effectiveness, and the possibility of complete oxidation of the pollutants (Iliuta and Iliuta, 2022). Numerous microorganisms have been identified for degrading cresol and phenol from contaminated waste water. The microorganisms, such as *Pseudomonas citronellolis* NS1 (Panigrahy et al., 2020), *Pseudomonas sp.* (Hamitouche et al., 2016), *Chlorella vulgaris* (Xiao et al., 2019), *Pseudomonas putida* (Surkatti and El-Naas, 2014), *Advenella sp*. LVX (Xenofontos et al., 2016), *Rhodococcus*, *Achromobacter*, PSB-M 3, and *Sphingobium* (Ailijiang et al., 2021) have been investigated for the degradation of phenolic com pounds. Usually, these bioremediation processes are carried out through two modes; (i) free cells and (ii) immobilized cells. The free cell system utilizes a suspension of microbial cells, whereas immobilized cells

refer to the microorganisms attached to porous support media. The free microbes have several disadvantages, such as losing microorganisms, toxic effects from high ambient concentrations and unpredictable microbial growth rates (Sonwani et al., 2019). The immobilization technology overcomes the disadvantages of the free cell system (Bao et al., 2021) by providing high removal efficiency of pollutants, chemical stability, and high biomass development in the face of adverse environmental circumstances (Maurya et al., 2022). Various researchers have observed that immobilizing the microbial cells in a suitable matrix can enhance the ability of microbial species to degrade organic pollutants during the bioremediation process (Shahabivand et al., 2022). The biodegradation of the phenolic compounds has been carried out in various attached growth bioreactors such as Packed Bed Bioreactors (PBBRS), Rotating Biological Contactors (RBCS), and Moving Bed Bio film reactors (MBBRS) (Swain et al., 2021). In attached growth bio reactors, the biodegradation process is greatly affected by the morphology, chemical constituents, and bioaffinity of the biocarriers. Therefore, in recent times, there has been significant interest in developing cost-effective, permeable, and durable biocarriers. Numerous carriers have been utilized to immobilize the microbes in this direction, including activated carbon (AC), sugarcane bagasse (SB), low-density polyethylene (LDPE), calcium alginate (CA), polyacrylamide, and polypropylene (PP), as well as polyurethane foam (PUF) (Ong et al., 2015). From the perspective of process engineering, PBBRs have numerous benefits, including high yield operation, convenience in scaling up, potential automation of separation processes leading to high degrees of purification, ability to treat large volumes of wastewater continuously by the specific number of immobilized cells, and the ability to reuse biomass (Banerjee and Ghoshal, 2016). Numerous studies have reported that immobilized cells in PBBRs can successfully biodegrade various harmful pollutants (Basak et al., 2019, Zhou and Nemati, 2018). Another benefit of PBBRs is the development of micro-niches with varying oxygen concentrations inside the supporting material's pores and within the layers of the biofilm (Martinkova et al., 2016). This study is focused on investigating the effects of process parameters such as, inoculum dose, pH of solution, and NaCl concentration on the specific growth of microbes. Furthermore, a comparative study of biodegradation of *p*-cresol was done in batch and continuous mode operation in RPBBR. Biodegradation kinetics was also evaluated. The effectiveness of RPBBR in terms of shock-loading of *p*-cresol and the metabolic pathway of the degraded sample were investigated. The bacterial toxicity assessment of the degraded products was also carried out.

4.2. Chemicals and methods

4.2.1. Mineral salt medium (MSM) and chemicals

In this present study, *p*-cresol (99%) and MSM (Mineral salt medium) were prepared as per the methods given in **Chapter 3 (Section 3.2.1)** in detail. Acclimatization, isolation and identification of *p*-cresol degrading pure strain have been discussed in previous studies (Jaiswal et al., 2023). Bacterial consortia (*Serratia marcescens* strain HL 1 and *Ochrobactrum intermedium* VrB9) were used in the biodegradation of *p*-cresol. The details of bacterial consortia have been discussed in the Appendix **(Appendix 4 (a)).**

4.2.2. Analytical methods

The concentration of bacterial cells and residual-cresol concentration were analysed as per the details given in **Chapter 3 (Section 3.2.4)**. Scanning electron microscopy (SEM) (Nova SEM 450, FEI, USA (S.E.A.) Pvt. Ltd., Singapore) was used after 15 days to evaluate the morphological characterization of the PUF carrier. GC–MS analysis employed (GC 7890B, 5977B GC/MSD) with HP- 5 MS column (30 m × 0.25 mm × 0.25 µm) containing FID detector and helium as carrier gas was used to perform the GC–MS analysis. The bioluminescence intensities of the treated, untreated, and control water samples were measured using a Horiba Fluorescence spectrophotometer (Model No.: PTI Quanta master TM 8000 series).

4.2.3. Process optimization for biodegradation of *p-cresol*

The process parameters, such as inoculum dose, pH, and NaCl concentration were optimized to enhance the specific growth and biodegradation of *p*-cresol. The inoculum of 2, 4, 6, 8, 10, 12, 14 and 16 (mL/100 mL) was varied. The optimum pH was determined by conducting experiments at various pH values (5, 6, 7, 8 and 9). The %NaCl was varied from 0.2 to 1.2 (w/100 mL). All the experiments were conducted at laboratory condition. The samples were collected at regular intervals to monitor bacterial growth.

4.2.4. Recirculating packed bed biofilm reactor

Recirculating packed bed biofilm reactor (RPBBR) was fabricated of borosilicate glass with a height of 60 cm and inner diameter of 5.5 cm, having a working capacity of approximately 1.2 L. Pre-sterilized PUF (1 cm × 1 cm × 1 cm) was used as the carrier for immobilization of bacterial

consortium due to its high porosity with strong resistance to water adsorption (Moghaddam et al., 2019). RPBBR was run for 15 days in batch mode. MSM as nutrient and *p*-cresol (50 mg L^{-1} to 100 mg L^{-1}) as carbon source were used under aerobic condition for the formation of biofilm on the carriers. A comparative study in batch mode has also been carried out with various concentrations of *p*-cresol (100 mg L^{-1} to 500 mg L^{-1}). All experiments were performed in triplicate. The constant volumetric flow rate of air (1 L min^{-1}) was maintained using rotameter (Flow point, India). A peristaltic pump (ELECTROLAB, PP- 50 V) was used to supply *p*-cresol solution at various flow rates to the reactor. pH and dissolved oxygen (DO) within the reactor was measured using pH meter (HD 2305.0; Delta OHM; Italy) and DO meter (HD 2109.1; Delta OHM; Italy) **(Fig. 4.1.),** respectively. The experiments were performed under laboratory condition.

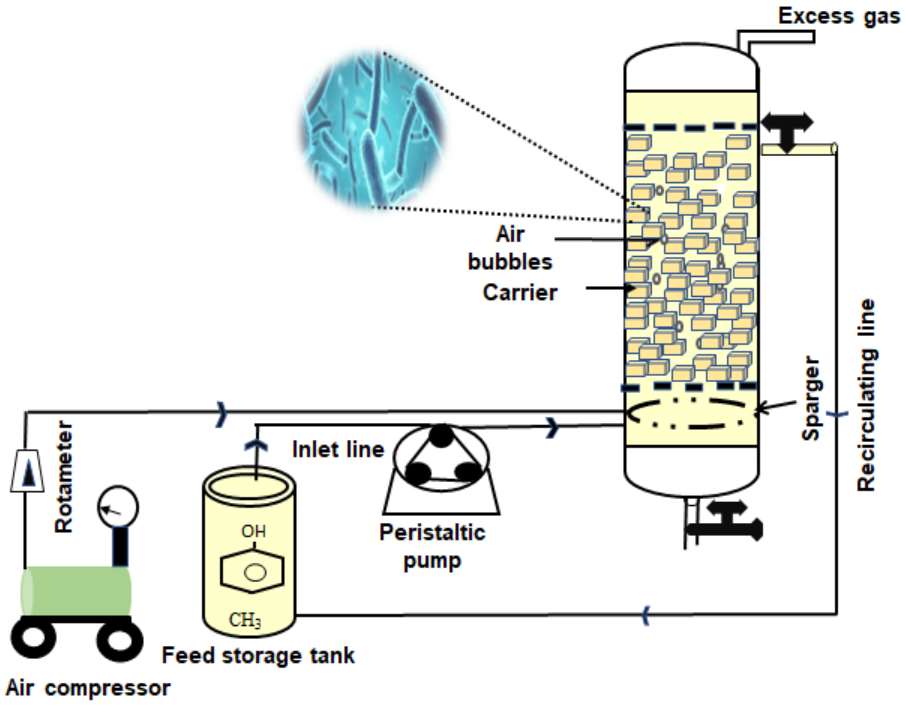

Fig. 4.1. Systematic diagram of recirculating packed bed biofilm reactor

4.2.5. Biodegradation kinetic model for *p*-cresol

The first-order kinetic model, **Eq. (4.1)** can be describe the biodegradation kinetics of hydrocarbons (Sharma and Pandey, 2022)

$$\frac{dC}{dt} = k_p \times C \quad \text{.....(4.1)}$$

Integrating **Eq. (4.1)**

$ln\frac{Co}{C} = k_p \times t$.....(4.2)

where k_p is first-order degradation constant, C_o is the initial concentration of *p*-cresol and C is the concentration of *p*-cresol at any time t = t

Biodegradation of *p*-cresol half-life calculated by using **Eq. (4.3)**

$t_{\frac{1}{2}} = \frac{0.69321}{k_p}$.....(4.3)

4.2.6. Identification of intermediate by-product using GC–MS technique

Biodegraded *p*-cresol was centrifuged (RM-12C BL) at 10,000 rpm for 10 min. The supernatant obtained after centrifugation was filtered using a 0.45 µm Whatman filter paper to remove the remaining cellular debris. Ethyl acetate was used to extract the metabolites after the supernatant was acidified (pH 2 with 0.5 M H_2SO_4) (Panigrahy et al. 2020). The metabolites of biodegraded *p*-cresol were extracted using ethyl acetate and followed by removing moisture in a rotary vacuum evaporator (IKA RV 10). The samples were diluted in chloromethane and used for GC–MS analysis. The temperature of the injector was kept between 25 °C and 300 °C. Injection of samples into the GC–MS was done at the split ratio 5:1.

4.2.7. Growth kinetics for biodegradation of *p*-cresol and bacterial toxicity assessment

The bacterial growth kinetics were analysed as per the details given in **Chapter 3 (Section 3.2.5)**. The bacterial toxicity of treated, untreated, and controlled sample were analysed as per the details given in **Chapter 3 (Section 3.3.6**)

4.3. Results and discussion

4.3.1. Biodegradation activity of single and consortium strain

p-Cresol degrading strains were isolated from the enriched sample using an enrichment approach. The two best *p*-cresol degrading strains were selected and used for consortium development based on their percentage removal efficiency of *p*-cresol **(Appendix 4 (b)).** It was observed that the percentage removal of the bacterial consortium was higher than the individual strain under the same condition **(Appendix 4 (b) Table 4 A).**

4.3.2. Effects of inoculum dose on specific growth

A sufficient amount of inoculum is necessary to reduce the period of the lag phase, accelerate the degradation rate, and initiate the exponential growth phase. The effect of inoculum dose on specific growth was illustrated in **Fig. 4.2.(a).** The specific growth of microbes continuously increases (0.04±0.0061 h^{-1} to 0.16±0.00502 h^{-1}) with an increase in inoculum dose (2 mL to 14 mL). Maximum growth (0.16 ±0.0052 h^{-1}) was evaluated at 14 mL of inoculum dose. However, with a further increase in inoculum dose (16 mL), the specific growth slightly decreases (0.16±0.0052 h^{-1} to 0.15±0.0024 h^{-1}). The decrease in specific growth might be due to decreased dissolved oxygen and increased competition for nutrients (Singh et al., 2022b).

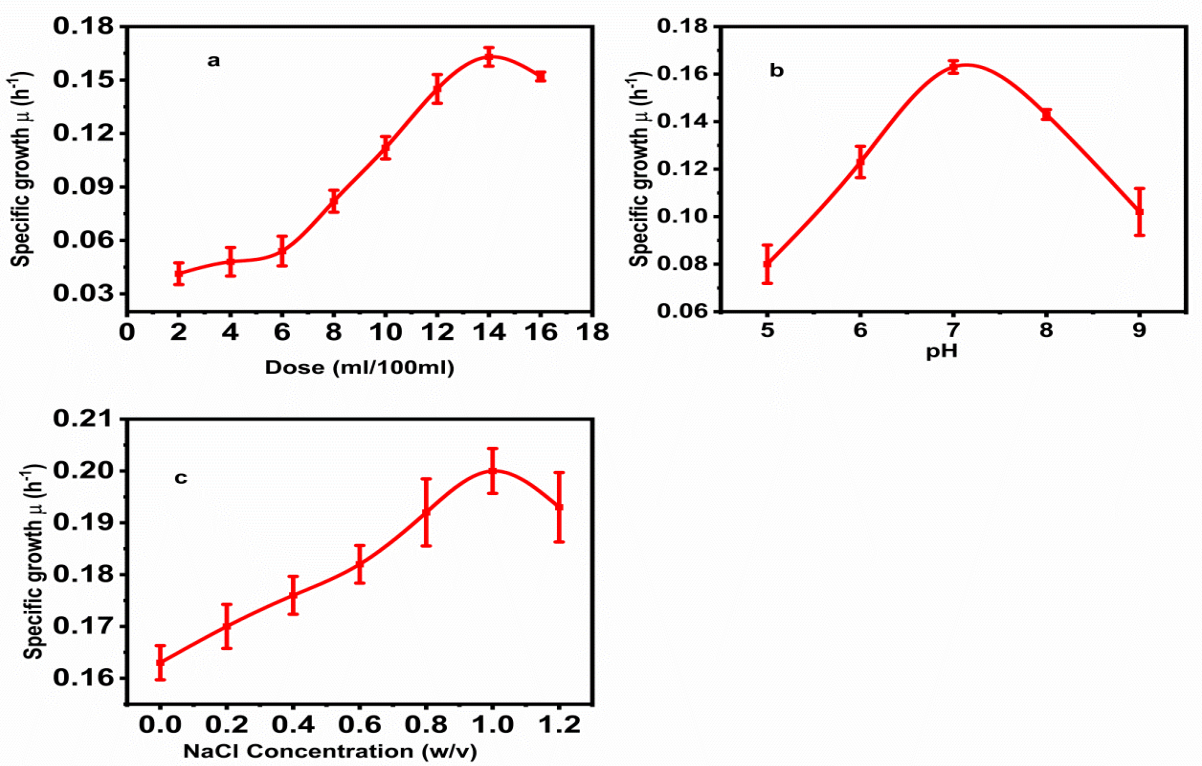

Fig. 4.2. Effect of bacterial consortia dose (a), pH (b), NaCl concentration (w/100mL), and (c) on specific growth of *p*-cresol biodegradation (100 mg L^{-1})

According to Sarkar and Dey (2020), increasing the inoculum dose reduces the lag period and accelerates biodegradation. Hence, 14 mL was the optimal inoculum dose for *p*-cresol biodegradation. High inoculant doses may alter bacterial features that affect the pollutant degradation rate (Yang et al., 2017). Furthermore, a higher inoculum dose (>14 mL) inhibited the microbial growth, which could be attributed to a decrease in dissolved oxygen and increased

competition for available resources (Eltoukhy et al., 2020). Xu et al. (2021) investigated the effects of inoculum dose (2%, 5%, 8%, 10%, 12% and 15%) on the biodegradation of phenol (500 mg L^{-1}) using the *Acinetobacter lwoffii* NL1 strain. Their finding shows that as the dose increases from 2% to 10%, the time required for phenol degradation decreased (20 h to 14 h). The results were attributed to an increase in inoculum dose, which accelerated the transition of bacteria into the exponential growth phase by shortening the lag phase.

4.3.3. Effects of pH on specific growth

pH is one of the primary elements affecting microbial growth and enzyme activity. Most of the enzymes of neutrophilic organisms tend to denature under severe pH and lose catalytic activity conditions (Bera et al., 2017). As a result, metabolic activities are inhibited, resulting in the instant death of biomass (Bera et al., 2017). An optimal pH is crucial for bacterial cells to consume the pollutant effectively. **Fig. 4.2.(b)** shows the variation in the specific growth of microorganisms according to different pH values. The maximum specific growth (0.163±0.052 h^{-1}) of microorganisms was found at pH 7. This suggests that the strain is a neutrophilic bacterium. Extreme pH can cause enzyme denaturation and loss of catalytic activity (Bera et al., 2019). An optimal starting pH must be maintained to successfully utilize *p*-cresol or any nutritional source. Hence pH 7 is optimal for the maximum specific growth of microorganisms.

4.3.4. Effects of NaCl concentration on specific growth

The effect of NaCl on the specific growth of microorganisms is illustrated in **Fig. 4.2.(c).** As the concentration of NaCl increases (0% to 1%), specific growth increases (0.163 h^{-1}±0.0052 to 0.20±0.0032h^{-1}) and found maximum at 1% of NaCl (w/ 100 mL). Furthermore, an increase in the concentration of NaCl from 1% to 1.2% leads to slightly decreased growth rate (0.20±0.0032 h^{-1} to 0.19±0.0067 h^{-1}). Higher specific growth at low amounts of NaCl (≤1g/100 mL) may be due to bacterial growth enhanced by a small amount of NaCl supplement. However, the decrease in specific growth suggested that microbial species might be stressed under high NaCl concentration, which reduces cellular activity (Jiang et al., 2017). Another study suggested that increased NaCl concentration above the optimal value may cause reduced bacterial metabolic activity that directly affects the growth of microorganisms due to plasmolysis, thus adversely affecting microbial activity (Li et al., 2019). According to Afzal et al. (2007), it has been

observed that a halophilic bacterial strain *Halomonas sp*. was able to degrade phenol present in saline industrial wastewater containing various concentrations (1% to 14% by weight) of sodium chloride. The study revealed that the most effective degradation of phenol occurred at an optimum concentration of 5% NaCl by weight.

4.3.5. Morphological analysis of packing material

Process variables such as pH, nutrition availability, substrate concentration, etc., affect how a biofilm develops on the medium (Sonwani et al., 2019). The metabolic activity of the bacteria and its extracellular compound are both necessary for the development of biofilm on the surface of the carrier (Wang et al., 2018). SEM **(Appendix 4 (c))** study of the carrier before bacterial immobilization (0^{th} day) confirmed the presence of micro-pores on the surface. After 15^{th} days, micro-pores were occupied microorganisms, a sign of biofilm forming on the carrier surface. The formation of thick bacterial biofilm on the surface and pores of PUF demonstrates the effective colonization of bacterial cells on carriers.

4.4. Comparative study of biodegradation of *p*-cresol in batch and continuous mode operation

The comparative study of biodegradation of *p*-cresol in batch and continuous mode operation was shown in **Fig. 4.3.** The removal efficiency continuously decreased (90.73±1.61% to 64.21±1.87%) as concentration increased (100 mg L^{-1} to 500 mg L^{-1}) in the batch mode operation. This decrease in % removal efficiency may be due to different inhibitory action of pollutants. Bera et al. (2019) utilized *Stenotrophomonas sp*. obtained from petroleum refinery wastewater for biodegradation of *p*-cresol and reported that 400 mg L^{-1} completely degraded within 189 h. The result reveals that the substrate consumption rate reduced with an increase in the initial concentration and resulted in a lowering of biodegradation due to the enhancement of *p*-cresol concentrations' inhibitory action. Furthermore, the performance of RPBBR was studied in continuous mode at fixed flow rate (2 mL min^{-1}). The removal efficiency of the continuous mode operation was 99.36±02% at 100 mg L^{-1} *p*-cresol. That is higher than the % removal in batch mode operation (100 mg L^{-1}). It is possible that effective mixing led to less mass transfer resistance, which is the cause of this improved degradation (Talha et al., 2018). The biodegradation process is high at low concentrations of *p*-cresol due to a fast sorption phase

caused by the physical-chemical interaction between the molecules and microbial cells wall (Surkatti and El-Naas, 2014). Meanwhile, further increase in the concentration of *p*-cresol (200 mg L^{-1} to 500 mg L^{-1}) % removal continuously decreased (91.91±1.91% to 71.38±1.87%), probably due to substrate inhibition. However, as substrate concentration increases, more time will be required for complete degradation (Swain et al., 2021). Similar results were obtained by Singh et al. (2008), who found how *Gliomastix indicus* degraded throughout a broad range of initial *p*-cresol concentrations (10 mg L^{-1} to 700 mg L^{-1}). They observed that as the initial concentration increased, the substrate consumption rate decreased because the substrate *p*-cresol increased the amount of inhibition.

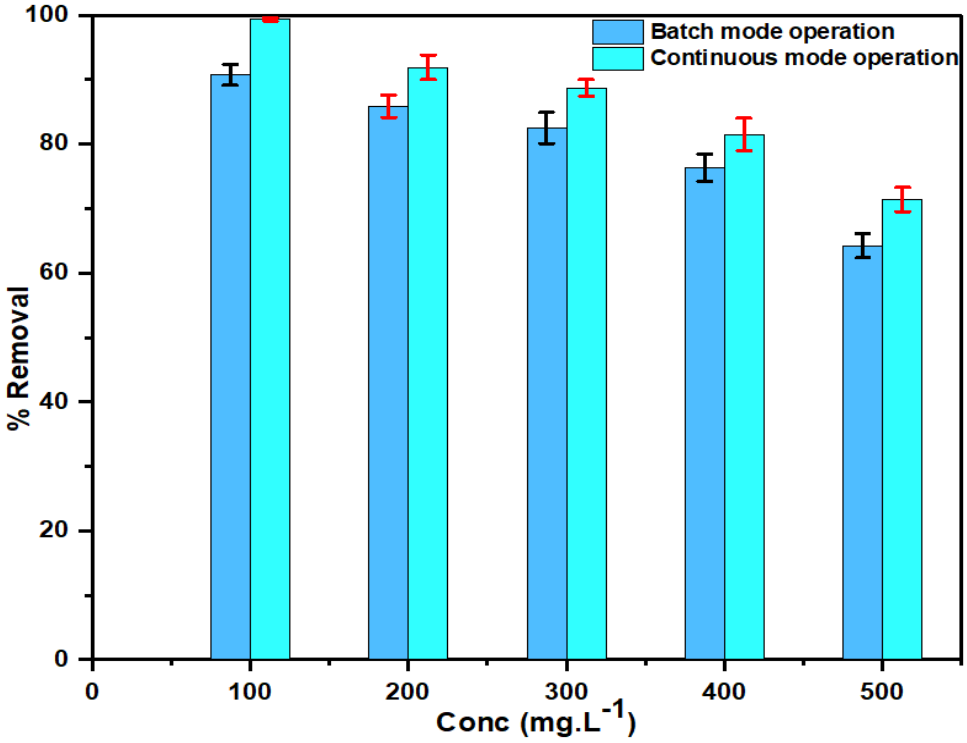

Fig. 4.3. Comparative study of biodegradation of *p*-cresol in batch and continuous mode operations for various *p*-cresol initial concentrations

4.4.1. First-order biodegradation kinetics

It assumed that the degradation kinetics relied on the degradation rate constant kp and the amount of active biomass. The amount of active heterotrophic biomass was expected to remain consistent throughout the experiment (Majewsky et al., 2011). The detailed first-order kinetics is illustrated in **Table 4.1** at optimized conditions.

Table 4.1 Summary of first-order rate constant and half-life for biodegradation of *p*-cresol

Initial concentration of *p*-cresol (mg L^{-1})	$ln\frac{C}{C_o}$ vs *t*	Rate constant k_p (day^{-1})	$t_{\frac{1}{2}}$ (day) 0.6932/(*k*)	R^2
Batch mode operation				
100	$ln\frac{C}{C_o}$ = 0.70t	0.7086	0.97	0.9884
200	$ln\frac{C}{C_o}$= 0.63t	0.6328	1.095	0.9653
300	$ln\frac{C}{C_o}$= 0.51t	0.5151	1.345	0.9594
400	$ln\frac{C}{C_o}$= 0.38t	0.3858	1.796	0.9537
500	$ln\frac{C}{C_o}$ = 0.31t	0.3129	2.215	0.9487
Continuous mode operation				
100	$ln\frac{C}{C_o}$= 0.96t	0.962	0.72	0.9818
200	$ln\frac{C}{C_o}$= 0.73t	0.7383	0.938	0.975
300	$ln\frac{C}{C_o}$= 0.72t	0.7208	0.96	0.9783
400	$ln\frac{C}{C_o}$= 0.52t	0.5281	1.31	0.9346
500	$ln\frac{C}{C_o}$= 0.40t	0.4093	1.69	0.9915

This experiment was carried out with increasing concentrations of *p*-cresol (100 mg L^{-1} to 500 mg L^{-1}) in batch and continuous mode operation. It was observed that *p*-cresol concentration affected the rate constant in batch and continuous medium operations. The maximum rate constant value for batch and continuous medium operation was 0.70 day^{-1} and 0.96 day^{-1}, respectively, for the initial 100 mg L^{-1} of *p*-cresol concentration. As concentration increased, the rate constant constantly decreased; consequently, the half-life increases. The decreased constant rate was due to the toxic effect of *p*-cresol. Tepe and Dursun, (2008) used *Ralstonia eutropha* for the biodegradation of phenol in batch-stirred and packed bed reactor with the assumption of first-order biodegradation kinetics, observed biodegradation rate constant was estimated at various flow rates. They found that the reaction rate decreases with the increased initial phenol concentration in both reactors and the maximum rate constant found in a continuous packed bed reactor.

4.4.2. Impact of shock loading of *p*-cresol on the performance of the RPBBR

The continuous operation of RPBBR is necessary for real operation. Effect of shock loading (different *p*-cresol concentration from 500 mg L^{-1} to 700 mg L^{-1}) and flow rate (5 mL min^{-1} to 55 mL min^{-1}) at fixed Retention time ((RT) =1 day) is demonstrated in **Fig. 4.4.**

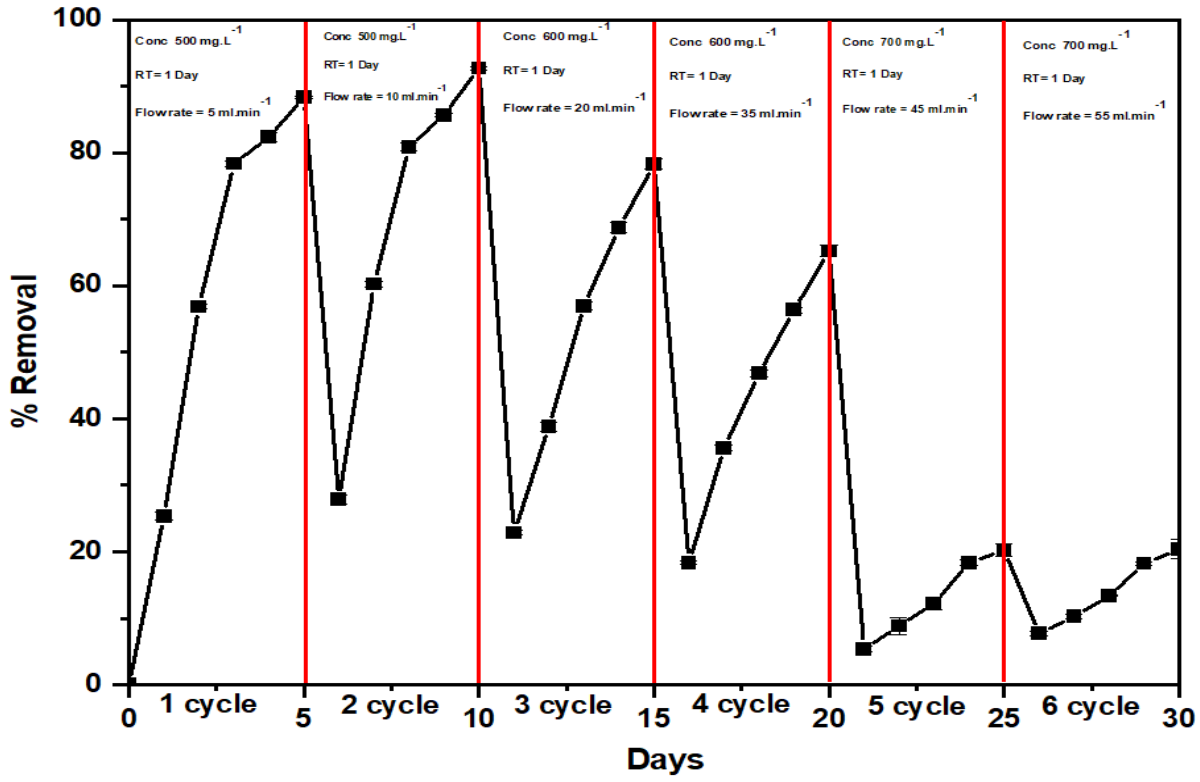

Fig. 4.4. Effect of shock disturbance on the performance of RPBBR for biodegradation of various concentrations of *p*-cresol and flow rate at constant retention time

The shock- loading operation included the six-cycle operating phases. The removal of *p*-cresol was influenced by both the flow rate and initial *p*-cresol concentrations. As flow rate increased from 5 mL min^{-1} to 10 mL min^{-1}, the removal efficiency increased from 88.38% to 92.72%, respectively after 1st cycle and initial concentration of 500 mg L^{-1}. However, the removal efficiency was decreased with increasing flow rate from 20 mL min^{-1} to 35 mL min L^{-1} at initial concentration of 600 mg L^{-1}. The performance of continuous bioreactor negatively affected against the high loading rate (Oberoi and Philip, 2017). The high flow rate led to the loss of more biomass and subsequently reduced the biodegradation efficacy (Surkatti and El-Naas, 2014). Similar kinds of effect were noticed for biodegradation Acid blue 113 dyes in fixed bed reactor by Tiwari et al. (2022).

4.4.3. FTIR analysis GC–MS analysis of biodegraded *p*-cresol

4.4.3.1. FTIR analysis of biodegraded *p*-cresol

The FTIR spectrum of biodegraded *p*-cresol solution was analyzed in the range of wave number 4000 cm^{-1} to 500 cm^{-1} (**Appendix 4 (d)).** The spectra at 3440 cm^{-1} reveals O-H shifting (He et al., 2021). The peak at 2979 cm^{-1} attributed to the presence of the methyl group. Similar findings relating to the existence of methyl group at wave number 2977-2979 cm^{-1} have been reported (Panigrahy et al., 2020). The band between 1700-1630 cm^{-1} is characterized by conjugate C=O and deconjugate C=O vibrations with aromatic or C=C elements (Zghari et al., 2017). The peak revealed the presence of methyl-substituted benzene derivatives detected at wave number 1385 cm^{-1}. This is strongly confirmed by the reported literature, which states that methyl-substituted benzene derivatives typically emerge in the 1415-1370 cm^{-1} range (Mathammal et al., 2016). The spectra that emerged at 1270 cm^{-1} and 1000 cm^{-1} revealed the existence of the C–O–C group. Similar trends for the presence of the C-O-C group have been reported for absorption spectra of 1260 cm^{-1} and 1080 cm^{-1} (Panigrahy et al., 2020).

4.4.3.2. Assessment of *p*-cresol biodegraded metabolic by-product using the GC-MS analysis

Several intermediate compounds closely connected to the biodegradation of *p*-cresol have been identified using GC–MS analysis. The mass spectra of the biodegradation of *p*-cresol comprised several fragmentation peaks **(Appendix 4 (e)).** The mass spectra obtained at m/z value of 125.0 demonstrated that the biodegraded product contained 4-methyl catechol (Panigrahy et al., 2020). However, a molecular ion peak at m/z 116.0 indicated maleic acid production. The presence of maleic acid at 116.0 m/z was also reported by Zakaria et al. (2020) during phenol degradation. Fragmented ion peak at 61.0 m/z supported glycerol synthesis in the *p*-cresol biodegradation pathway. The metabolic products involved in the biodegradation of *p*-cresol could not be identified in the current investigation, especially those at very low concentrations where a high noise-to-signal ratio may have contaminated the mass spectra, making them difficult to interpret. A metabolic pathway for the biodegradation of *p*-cresol is proposed **(Appendix 4 (f)).**

4.4.3.3. Bacterial toxicity assessment using *Pseudomonas fluorescens*

The bioluminescence intensity of *Pseudomonas fluorescens* (*P.f.*) was used to evaluate the bacterial toxicity of *p*-cresol in WD and degraded in RPBBR through continuous and batch systems. *P.f.* bioluminescence intensity was found to be lower (2.78×10^6 counts per second) in WD sample than the control sample (distilled water) (11.74×10^6 second). However, the bioluminescence intensity was higher for treated wastewater in CS (5.4×10^6 counts per second) and BS (4.2×10^6 per second) systems than WD sample **(Appendix 4 (g)).** This leads to more mineralization of *p*-cresol in a continuous system. A similar phenomenon was observed under long time exposure (24 h, chronic effects) to degrade *p*-cresol in continuous and batch system **(Appendix 4 (h)).** The WD *p*-cresol sample exhibited 76.66±1.8 % and 86.82±1.62 % P.f. bioluminescence intensity during acute and chronic toxicities, respectively **(Appendix 4 (g), (h)).** *P.f.* bioluminescence intensity in the continuous system for acute and chronic exposure was obtained to be 53.66±1.2% and 59.47±1.3%, respectively. Similarly, the *P.f.* bioluminescence intensity for *p*-cresol degraded in the batch system for acute and chronic exposure was found to be 63.54±2.32% and 67.78±2.15%, respectively **(Appendix 4 (i)).**

4.5. Conclusions

The effect of inoculum, pH, and NaCl% on specific growth was studied to achieve the maximum degradation of *p*-cresol from waste water. The maximum efficiency of 99.36±0.2% was obtained at 100 mg L^{-1} of initial *p*-cresol concentration. Biodegradation of *p*-cresol followed the first-order kinetics. The performance of RPBBR was adversely affected under high shock-loading rate. During the biodegradation of *p*-cresol, the intermediates identified as maleic acid, glycerol, and 4-methyl catechol. Bacterial toxicity assessment ensures the mineralization of *p*-cresol. RPPBR may be explored further in the secondary stage of wastewater treatment plants (i.e., biological processes) to treat a wide range of pollutants.